ORIGINAL RESEARCH

DOCK2 Promotes Pleural Fibrosis by Modulating Mesothelial to Mesenchymal Transition

Guoqing Qian[1], Oluwaseun Adeyanju[1], Saptarshi Roy[1], Christudas Sunil[1], Ann Jeffers[1], Xia Guo[1], Mitsuo Ikebe[1], Steven Idell[1,2], and Torry A. Tucker[1,2]

[1]Department of Cellular and Molecular Biology, The University of Texas Health Science Center at Tyler, Tyler, Texas; and [2]The Texas Lung Injury Institute, Tyler, Texas

ORCID ID: 0000-0003-1804-7993 (G.Q.).

Abstract

Mesothelial to mesenchymal transition (MesoMT) is one of the crucial mechanisms underlying pleural fibrosis, which results in restrictive lung disease. DOCK2 (dedicator of cytokinesis 2) plays important roles in immune functions; however, its role in pleural fibrosis, particularly MesoMT, remains unknown. We found that amounts of DOCK2 and the MesoMT marker α-SMA (α-smooth muscle actin) were significantly elevated and colocalized in the thickened pleura of patients with nonspecific pleuritis, suggesting the involvement of DOCK2 in the pathogenesis of MesoMT and pleural fibrosis. Likewise, data from three different pleural fibrosis models (TGF-β [transforming growth factor-β], carbon black/bleomycin, and streptococcal empyema) consistently demonstrated DOCK2 upregulation and its colocalization with α-SMA in the pleura. In addition, induced DOCK2 colocalized with the mesothelial marker calretinin, implicating DOCK2 in the regulation of MesoMT. Our *in vivo* data also showed that DOCK2-knockout mice were protected from *Streptococcus pneumoniae*–induced pleural fibrosis, impaired lung compliance, and collagen deposition. To determine the involvement of DOCK2 in MesoMT, we treated primary human pleural mesothelial cells with the potent MesoMT inducer TGF-β. TGF-β significantly induced DOCK2 expression in a time-dependent manner, together with α-SMA, collagen 1, and fibronectin. Furthermore, DOCK2 knockdown significantly attenuated TGF-β–induced α-SMA, collagen 1, and fibronectin expression, suggesting the importance of DOCK2 in TGF-β–induced MesoMT. DOCK2 knockdown also inhibited TGF-β–induced Snail upregulation, which may account for its role in regulating MesoMT. Taken together, the current study provides evidence that DOCK2 contributes to the pathogenesis of pleural fibrosis by mediating MesoMT and deposition of neomatrix and may represent a novel target for its prevention or treatment.

Keywords: DOCK2; lung; pleural fibrosis; mesothelial to mesenchymal transition; TGF-β

Pleural fibrosis is characterized by early pleural inflammation with subsequent organization and thickening of the pleura. This reorganization leads to remodeling of the lung architecture and subsequent impairment of lung function. Pleural fibrosis frequently occurs as a result of complications of a range of pulmonary parenchymal diseases including pneumonia with parapneumonic effusion or empyema, tuberculosis, hemothorax, and asbestos-related pleural disease or treatments including drugs (e.g., ergot drugs) and thoracic irradiation (1, 2). Currently, there is no effective treatment for this disease, mandating better understanding of the process.

Over the years, many *in vivo* models of pleural fibrosis have been developed to recapitulate the human pathological processes, including the use of carbon black/bleomycin (CBB) (3, 4), TGF-β (transforming growth factor-β) (5), and *Streptococcus* infection (6). In particular, these studies implicate the involvement of TGF-β and other factors in the progression of pleural scarification. Increasing evidence supports an important role of mesothelial

(Received in original form April 12, 2021; accepted in final form October 26, 2021)

Supported by Foundation for the National Institutes of Health grants HL130133 (T.A.T.), HL141583 (X.G.), and HL142853 (M.I., S.I., and T.A.T.) and the University of Texas Health Science Center at Tyler Startup fund (G.Q. and X.G.).

Author Contributions: G.Q. as the corresponding author codesigned the research with X.G. and S.I. S.I. and T.A.T. provided cells and tissues. G.Q., O.A., S.R., C.S., A.J., and X.G. performed the experiments. G.Q. wrote the manuscript. G.Q. and X.G. analyzed the data. M.I. provided experimental design support. X.G., M.I., S.I., and T.A.T. contributed comments on the manuscript.

Correspondence and requests for reprints should be addressed to Guoqing Qian, Ph.D., Department of Cellular and Molecular Biology, University of Texas Health Science Center at Tyler, 11937 US Highway 271, Lab-A1, Tyler, TX 75708. E-mail: guoqing.qian@uthct.edu.

This article has a related editorial.

This article has a data supplement, which is accessible from this issue's table of contents at www.atsjournals.org.

Am J Respir Cell Mol Biol Vol 66, Iss 2, pp 171–182, February 2022

Originally Published in Press as DOI: 10.1165/rcmb.2021-0175OC on October 28, 2021
Internet address: www.atsjournals.org

cells in the development of pleural fibrosis (7, 8). Whereas persistent injuries may lead to cellular apoptosis, the mesothelial to mesenchymal transition (MesoMT) of resident pleural mesothelial cells (PMCs) contributes to cellular activation and proliferation. This process is likewise characterized by increased α-SMA (α-smooth muscle actin) expression, as well as increased extracellular matrix including collagen and fibronectin (FN) (9, 10). These products contribute to the development of pleural fibrosis. We have reported that many mediators promote MesoMT, including TGF-β, plasmin, urokinase-type plasminogen activator (uPA) (4), factor Xa (11), and thrombin (12, 13). Among these, TGF-β is the most potent profibrotic factor. Inhibition of Smad, PI3K, NF-κB, and GSK-3β signaling have been found to abrogate or attenuate TGF-β–induced MesoMT *in vitro* and pleural fibrosis *in vivo* (13–15). These studies provide insight into the cross-talk among different signaling pathways in the development of pleural fibrosis. TGF-β signaling has been shown to activate several important transcription factors including *Snail* to induce myofibroblast differentiation (16, 17). However, little is known about the function of these transcription factors in MesoMT.

DOCK2 (dedicator of cytokinesis 2) belongs to the large DOCK family of *Drosophila melanogaster* myoblast city (CDM) proteins. Under physiological conditions, DOCK2 is expressed specifically in hematological cells (18). The diverse roles of DOCK2 in regulating lymphocyte migration, chemoattraction, and proliferation largely depend on its Rac activating function (19–21). Previously, we reported that DOCK2 was induced during vascular injury and contributed to the regulation of smooth muscle phenotype during vascular remodeling after injury (22). A recent paper shows that DOCK2 is involved in macrophage activation in response to LPS- and endotoxemia-induced acute lung injury in mice that is associated with its role in promoting inflammation (23). DOCK2 has also been shown to modulate cell phenotype and to be remarkably induced by proinflammatory cytokines, including TNF-α, IL-1β, and platelet-derived growth factor (PDGF) (22, 24), which are also considered to play a role in the pathogenesis of pleural fibrosis. However, little is known about the role and function of DOCK2 in the pathogenesis of pleural fibrosis, which forms the predicate for the current study.

Here, we report the novel observation that mesothelial cell expression of DOCK2 in human and murine models of organizing pleural injury contributes to the pathogenesis of pleural fibrosis. Whereas TGF-β significantly enhanced DOCK2 expression in primary human PMCs (HPMCs), DOCK2 knockdown attenuated TGF-β–induced MesoMT in HPMCs, suggesting that DOCK2 contributes to TGF-β signaling in pleural fibrosis.

Methods

Human Nonspecific Pleuritis Lung Tissues

The collection and availability of human nonspecific pleuritis lung tissues and controls were reported previously (5). Human pleural tissues were obtained from the National Disease Research Interchange. These tissues were from surgical biopsies or autopsy specimens from patients with pneumonia and a clinical diagnosis of nonspecific pleuritis or from patients with histologically near-normal pleural tissues who died of causes otherwise unrelated to any pleural pathological process.

Animal Models

The CBB-induced pleural fibrosis model was described previously (4). Briefly, anesthetized C57BL/6 mice were intrapleurally injected with 100 μl of a CBB mixture (0.1 mg carbon black/0.07 U bleomycin) in 0.9% saline. Control group mice were intrapleurally injected with 100 μl of 0.9% saline. Pleural injury was examined at 14 days after treatment. The *Streptococcus pneumoniae*–induced empyema model was described previously (6). Briefly, wild-type (WT) C57BL/6 mice and DOCK2-knockout mice (22, 25) were intrapleurally administered *S. pneumoniae* (D39, 1.8×10^9 cfu) in saline or saline alone, as a control. One week after administration, lung volume and function (compliance) were determined using Micro CT and flexiVent, respectively, followed by the collection of lung tissues for histochemical analyses. All animal experiments were approved by the Institutional Animal Care and Use Committee at the University of Texas Health Science Center at Tyler.

Cell Culture and Treatment

Isolation and culture of HPMCs in this study were described previously (5, 13, 26). HPMCs were collected from pleural effusions of patients experiencing congestive heart failure or coronary artery bypass graft surgery. Pleural fluid collection was approved through an exempt protocol by the Institutional Human Subjects Review Board of the University of Texas Health Science Center at Tyler. The cells were cultured in LHC-8 medium (Life Technologies) supplemented with 3% FBS, 2% antibiotic-antimycotic, and 1% GlutaMAX in a humidified incubator at 37°C with 5% CO_2, as previously reported. Cells were starved in serum-free RPMI-1640 medium supplemented with GlutaMAX, followed by stimulation with recombinant human TGF-β (R&D Systems). Actinomycin D (Act D) purchased from MilliporeSigma was used as a transcription inhibitor (27). The DOCK2-Rac inhibitor CPYPP (28) was purchased from MedChemExpress.

Western Blotting

Whole-cell lysates were collected in radioimmunoprecipitation assay (RIPA) lysis buffer from cells after treatments. Total protein concentrations were measured using the BCA (bicinchoninic acid) protein assay kit, according to manufacturer's guide. Equal amounts of total protein (10–20 μg) were denatured using Laemmli SDS buffer and loaded for SDS-PAGE gel electrophoresis. Proteins were transferred to PVDF membranes, which were blocked with 5% milk, and then incubated with primary antibodies at 4°C overnight. The primary antibodies used were as follows: DOCK2 (Cat#09-454; MilliporeSigma), α-SMA (Clone 1A4; Sigma-Aldrich), collagen 1 (Col-1, Cat#1310-08; SouthernBiotech), FN (Cat#ab2413; Abcam), and GAPDH (Clone 1E6D9; Proteintech).

Quantitative Real-Time PCR Analysis

The detailed method has been reported previously (29). Briefly, total RNA was collected into Trizol, and then, 1 μg of total RNA was reverse transcribed into cDNA using a reverse transcription kit from BioRad. Diluted cDNA templates were used for quantitative real-time PCR (qPCR) analysis of gene expression using SYBR green from BioRad. *GAPDH* was used as the internal control. The primers of genes used are shown in Table E1 in the data supplement.

Lung Histology, Morphometry, and Immunohistochemical Staining

Formalin-fixed and paraffin-embedded slides were used for lung histology, morphometry, and immunohistochemical (IHC) staining of DOCK2. Collagen deposition and morphometric alterations were assessed by Masson's trichrome staining, as previously described (4). Pleural tissue thickness was measured by morphometry as previously reported (4). The slides underwent typical steps of dewaxing in xylene, rehydration, and antigen retrieval; 3% H_2O_2 quenching of endogenous peroxidase activity; and then blocking with 10% goat serum in PBS, followed by incubation with primary anti-DOCK2 antibody (1:100) overnight at 4°C. After washing with PBS three times, the slides were then incubated with secondary anti-rabbit horseradish peroxidase (1:100; Invitrogen) for 1 hour at room temperature. 3, 3'-diaminobenzidine (DAB) staining was performed according to the manufacturer's guide and examined under light microscope until proper staining developed.

Immunofluorescence Staining

Formalin-fixed and paraffin-embedded slides were routinely processed similarly to that of IHC procedures, proceeding to primary antibody incubation overnight at 4°C. The primary antibodies used were DOCK2 (Cat#09-454; MilliporeSigma; and E7; Santa Cruz) and α-SMA (Cat#A2547; MilliporeSigma) and calretinin (Cat#C7479; MilliporeSigma). Secondary antibodies used were goat anti-mouse Alexa Fluor Plus 488 (Cat#A32723; Invitrogen), goat anti-rabbit Alexa Fluor Plus 488 (Cat#A32731; Invitrogen), goat anti-mouse Texas Red (Cat#2015320; Invitrogen), and goat anti-rabbit Texas Red (Cat#2015320; Invitrogen). The images were taken using a Nikon NiU microscope.

Adenovirus Infection and siRNA Transfection

Control or shRNA targeting DOCK2 (shDOCK2) using adenovirus have been reported previously (22). Briefly, cells in a 6-well plate (~50–70% confluency) were infected with control or shDOCK2 adenovirus in 2 ml of complete LHC-8 growth medium for 6 hours, followed by removal of medium and replacement with fresh complete growth medium for culture overnight. Cells were then starved in serum-free RPMI-1640 medium for an additional 24 hours, followed by the addition of TGF-β in starve medium for different doses or time points as indicated in the results. Control siRNA (SIC001; MilliporeSigma) and siRNA targeting *Snail* (SASI_Hs01_00039785; MilliporeSigma) were transfected using jetPRIME from Polyplus-transfection according to the manufacturer's protocol.

Pulmonary Function Testing

Pulmonary function testing was performed as previously described (4, 30). Briefly, mice were anesthetized with a ketamine and xylazine mixture and intubated with a 20-gauge sterile intravenous cannula (EXE 26741; Thermo Fisher Scientific) between the vocal cords into the trachea. Mice were maintained under anesthesia using isoflurane during pulmonary function testing of compliance, which was determined by the "snapshot perturbation method" according to the manufacturer's guide.

Lung Volume Measurements by Computed Tomography

Computed tomography (CT) scan and lung volume measurements we used have been reported previously (4, 30). Ketamine and xylazine-anesthetized mice were sedated further by supply with an isoflurane and oxygen mixture to minimize spontaneous breaths during chest CT scan and pulmonary function testing. CT scan images were generated using the eXplore Locus micro–computed tomography (Micro CT) Scanner. Lung volumes were measured from renditions collected at full inspiration using the MicroView software that produces three-dimensional images and calculates volumes.

Statistical Analysis

Comparisons between two groups were conducted using Student's *t* test. Multiple comparisons were conducted using one-way ANOVA followed by Dunnett's method. All the analyses were performed using GraphPad Prism Software. Data are shown as mean ± SD. A *P* value less than 0.05 was considered statistically significant.

Results

DOCK2 Expression Is Induced in Pleural Fibrosis

Patients with pleuritis may develop subsequent fibrosis because of prolonged inflammation and remodeling of the peripheral lung and pleural surfaces. To determine whether DOCK2 was involved in human pleural fibrosis, we checked DOCK2 expression in the lung tissues of patients who had nonspecific pleuritis and normal controls lacking any clinically apparent pleural injury ($n = 3$ per group). Hematoxylin and eosin staining showed dramatic remodeling of the lung in patients with nonspecific pleuritis as well as thickening of the mesothelium (Figure 1A), suggesting the activation and expansion of the mesothelial cells. Extensive fibrosis was present in the visceral pleural layer and subpleural areas as indicated by strong deposition of collagen in nonspecific pleuritis lung tissues (blue stain, Figure 1B) compared with the thin layer of mesothelial cells in the normal control lung. Furthermore, we found significantly increased DOCK2 expression ($P < 0.001$) in the visceral pleura of patients with nonspecific pleuritis versus those of normal control patients, as shown by immunofluorescence (IF) staining (Figure 1C). These data demonstrate that DOCK2 expression is locally enhanced in organizing pleural injury in human lung tissues.

Elevated DOCK2 Expression at the Pleural Mesothelial Layer in Preclinical Models of Pleural Injury

Experimental models of pleural injury characterized by fibrotic repair were next employed to understand the pathogenesis of pleural thickening and fibrosis. Previously, we have shown that TGF-β, CBB, and *S. pneumoniae*–induced pleural injury promote pleural fibrosis in the lungs of C57BL/6 mice (4–6, 13). Using archived lung tissues (Figure 2), we confirmed that pleural injury caused by intrapleural injuries locally induced by TGF-β, CBB, and *S. pneumoniae* caused notable pleural thickening (Figures 2A–2C) and increased collagen deposition in the mesothelial layer (Figures 2D–2F). Furthermore, we demonstrated that DOCK2 expression was remarkably induced in the lung mesothelial surface, as shown by IHC staining in these different models (Figures 2G–2I). A time-dependent induction of DOCK2 was also noted in the *Streptococcus* empyema model (*see* Figure E1). These data show that DOCK2 is commonly induced in disparate preclinical models of pleural fibrosis.

Colocalization of DOCK2 and Mesenchymal Marker α-SMA in Pleural Fibrosis *In Vivo*

MesoMT is crucial for the development of pleural fibrosis (31). Furthermore, inhibition of MesoMT has been shown to block pleural

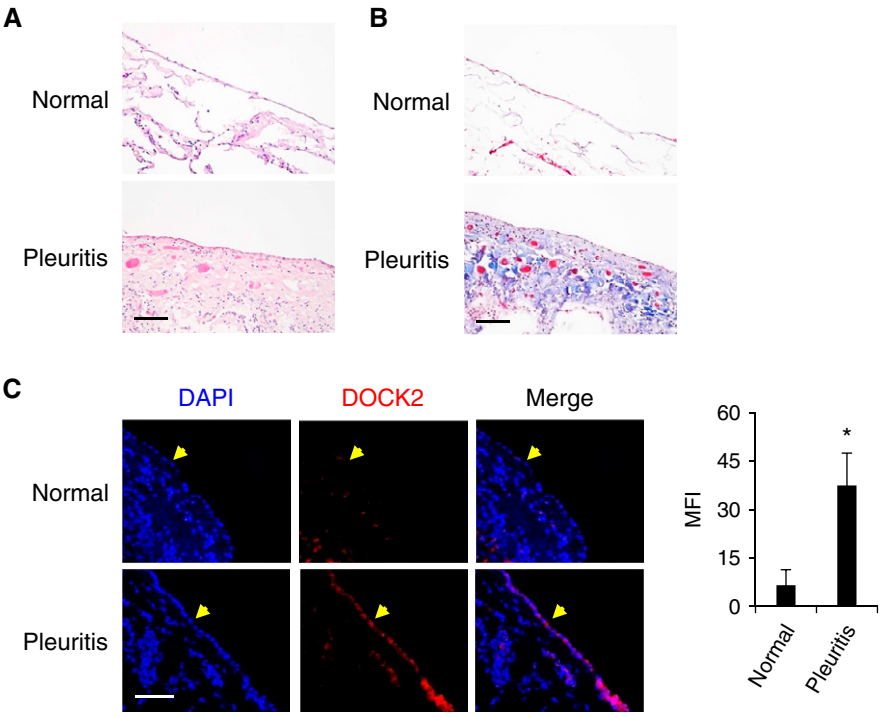

Figure 1. DOCK2 (dedicator of cytokinesis 2) expression was induced in human pleural fibrosis. (*A*) Hematoxylin and eosin staining in human normal and pleuritis lung suggested increased fibrosis in the visceral pleura of a patient with nonspecific pleuritis versus that in a normal control patient. Findings are representative of $n = 5$ per each group. (*B*) Masson's trichrome staining of collagen staining showed the remodeling of the lung with pleural fibrosis associated with nonspecific pleuritis (findings representative, $n = 5$ per group). (*C*) Representative immunofluorescence (IF) staining showed increased DOCK2 (red) expression in the lung of patients with pleuritis. DAPI stained the nuclei (blue). Arrowheads indicated the DOCK2 (red) expression that appeared to be located in the mesothelial surface of the pleural tissues of patients with nonspecific pleuritis. Scale bars, 100 μm.Images are representative of the findings of 10 fields per slide and five patients per group. *$P < 0.05$ compared with normal control patients. MFI = mean fluorescence intensity.

fibrosis associated with TGF-β adenovirus transduction (5) and *S. pneumoniae* infection (5, 15). To assess the possible role of DOCK2 in MesoMT, we next determined whether DOCK2 expression colocalizes with the MesoMT marker α-SMA using IF staining. Consistent with the results shown in Figure 1C, we found in patients with nonspecific pleuritis that both α-SMA and DOCK2 expression was increased at the pleural surface, where these two proteins colocalized well (Figure 3A). In addition, IF staining showed that DOCK2 expression was dramatically induced at the visceral pleura of mice treated with CBB for 14 days (Figure 3B) or *S. pneumoniae* for 14 days (Figure 3C), which colocalized with the MesoMT marker, α-SMA, at the pleural surface. These *in vivo* data support the concept that DOCK2 may regulate MesoMT in the context of pleural fibrosis.

DOCK2 Expression Colocalizes with the Mesothelial Marker Calretinin *In Vivo*

Calretinin, an established marker of mesothelial cells (4, 32), was used to determine whether upregulated DOCK2 was localized to the PMCs. Fibrotic pleural tissues induced by CBB and *S. pneumoniae*, respectively, were subjected to IF analysis for calretinin and DOCK2. A thin layer of calretinin staining, but no DOCK2 at the mesothelial surface, was observed in the control saline group. In contrast, both CBB (Figure E2A) and *S. pneumoniae* (Figure E2B) treatment induced thickening of the mesothelial layer, which was characterized by increased calretinin staining. DOCK2 expression was likewise induced dramatically in the pleural mesothelium, which showed colocalization with calretinin. The negative control using normal rabbit IgG and corresponding secondary fluorescent antibody on saline- or CBB-treated mouse lung tissues was included but showed no staining of calretinin or DOCK2 (Figure E3). Together, the data confirm that DOCK2 is enhanced in mesothelial cells in organizing pleural fibrosis.

DOCK2-Knockout Mice Are Protected from *S. pneumoniae*–induced Pleural Fibrosis

To determine the role of DOCK2 in pleural fibrosis development and progression, we administered *S. pneumoniae* or saline to WT and DOCK2-knockout mice (on a C57BL/6 background) mice to assess pleural fibrosis. This model was chosen for these experiments given that pleural organization after bacterial infection is strongly related to outcomes (8). We found that *S. pneumoniae* induced DOCK2 expression in the mesothelium of WT mice but not in the DOCK2-knockout mice, indicating specificity of DOCK2 staining (*see* Figure E4A). *S. pneumoniae* significantly decreased lung volume and decreased lung compliance in WT mice. In contrast, no evident or significant decrements in lung function and volume were observed in DOCK2-knockout mice receiving *S. pneumoniae*; compared with WT mice treated *S. pneumoniae*, the DOCK2 knockout receiving *S. pneumoniae* showed significantly greater lung volume and compliance (Figures 4A and 4B). Furthermore, collagen deposition was prominent in the thickened pleural layer in *S. pneumoniae*–treated WT mice but not in DOCK2-knockout mice (Figure 4C). Accordingly, pleural thickness in WT mice was significantly increased by *S. pneumoniae*. Conversely, *S. pneumoniae*–injured DOCK2-knockout mice demonstrated significantly less pleural thickness than WT mice ($P < 0.05$, Figure 4D). The MesoMT marker α-SMA was likewise increased in *S. pneumoniae*–injured WT mice, whereas DOCK2-knockout mice demonstrated little to no induction of α-SMA in the pleural layer (Figure 4E). In addition, we conducted IHC staining of α-SMA and Col-1 in the pleura of WT and DOCK2-knockout mice that received saline or *S. pneumoniae* (*see* Figures E4B and E4C). Consistent results were observed by trichrome staining (Figure 4C) and IF staining (Figure 4E). These findings together support a critical role for DOCK2 in the development of pleural fibrosis through mediating MesoMT.

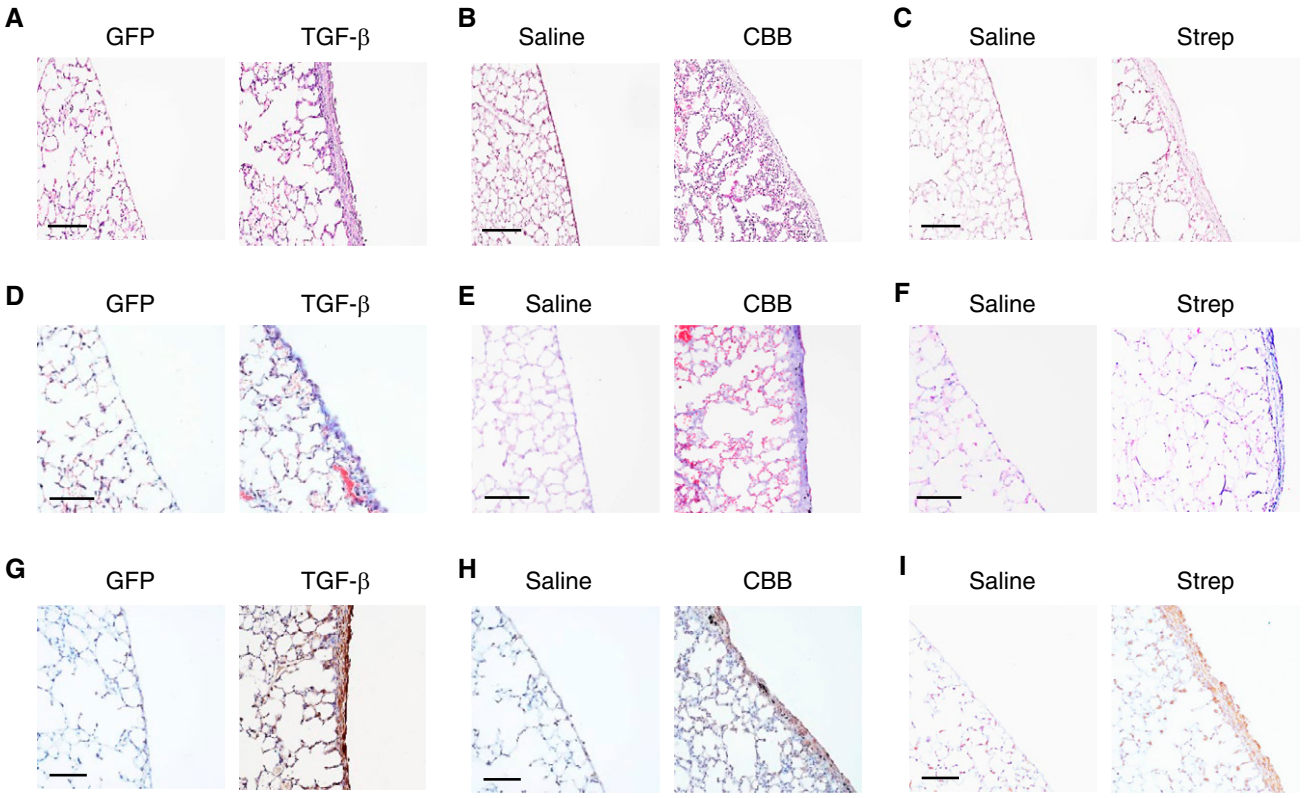

Figure 2. DOCK2 expression was increased in the lung with induced pleural fibrosis *in vivo*. (*A–C*) Hematoxylin and eosin staining showed thickening of lung pleural layer of C57BL/6 mice treated with TGF-β (transforming growth factor-β) (7 days) (*A*), carbon black/bleomycin (CBB) (14 days) (*B*), and *S. pneumoniae* (Strep) (14 days) (*C*). (*D–F*) Masson's trichrome staining showed induced pleural fibrosis in the lung of C57BL/6 mice treated with TGF-β (7 days) (*D*), CBB (14 days) (*E*), and Strep (14 days) (*F*). (*G–I*) Immunohistochemical staining showed increased DOCK2 expression in the fibrosis layer of the lung of C57BL/6 mice treated with TGF-β (7 days) (*G*), CBB (14 days) (*H*), and Strep (14 days) (*I*). Scale bars, 100 μm.

TGF-β Induces DOCK2 Protein Expression in HPMCs

To extend the findings in human nonspecific pleuritis and preclinical models, we performed *in vitro* experiments using HPMCs treated with the potent MesoMT inducer TGF-β. We found that the basal amount of DOCK2 protein expression was relatively low in HMPCs but was significantly increased by TGF-β ($P < 0.05$, Figures 5A and 5B). TGF-β likewise increased the expression of MesoMT markers, α-SMA, Col-1, and FN. Because 5 ng/ml TGF-β maximally induced the expression of DOCK2 and MesoMT markers, it was used for all subsequent *in vitro* experiments. DOCK2 expression was also induced by TGF-β in a time-dependent manner and was significantly increased after 8 hours through 24 hours (Figures 5C and 5D). MesoMT markers α-SMA, Col-1, and FN were also significantly increased in a time-dependent manner, with dramatic increases (greater than twofold) occurring after 8 hours. Similar results were found in parallel studies using different lines of HPMCs (Figures 5E and 5F). Taken together, the data show TGF-β induces DOCK2 expression in a time- and dose-dependent manner. These data furthermore suggest that DOCK2 may play a role in TGF-β–induced MesoMT.

TGF-β Induces DOCK2 Expression at the Transcriptional Level

To further explore DOCK2 induction by TGF-β, we performed qPCR analyses of DOCK2 mRNA in HPMCs after treatment with TGF-β for different doses and times. We found that DOCK2 mRNA was significantly induced in a dose- and time-dependent manner in two primary HPMCs lines (Figures 6A–6D). To determine the contribution of transcriptional regulation on DOCK2 expression, the transcription inhibitor Act D was used. TGF-β–induced DOCK2 expression was significantly blocked by Act D at both the mRNA (Figure 6E) and the protein level (Figure 6F). These studies confirmed that DOCK2 was induced by TGF-β at the transcriptional level in HPMCs.

DOCK2 Is Required in TGF-β–induced MesoMT in HPMCs

To determine DOCK2's role in TGF-β–induced MesoMT, we knocked down DOCK2 using adenoviral shRNA in HPMCs and then stimulated serum-starved HPMCs with TGF-β. In vector controls, TGF-β significantly induced expression of MesoMT markers α-SMA, Col-1, and FN. In contrast, DOCK2 downregulation significantly attenuated/blocked the induction of α-SMA, Col-1, and FN by TGF-β in HPMCs (Figures 7A and 7B), indicating that DOCK2 is required in TGF-β–induced MesoMT. We next tested whether the DOCK2-Rac activity is required

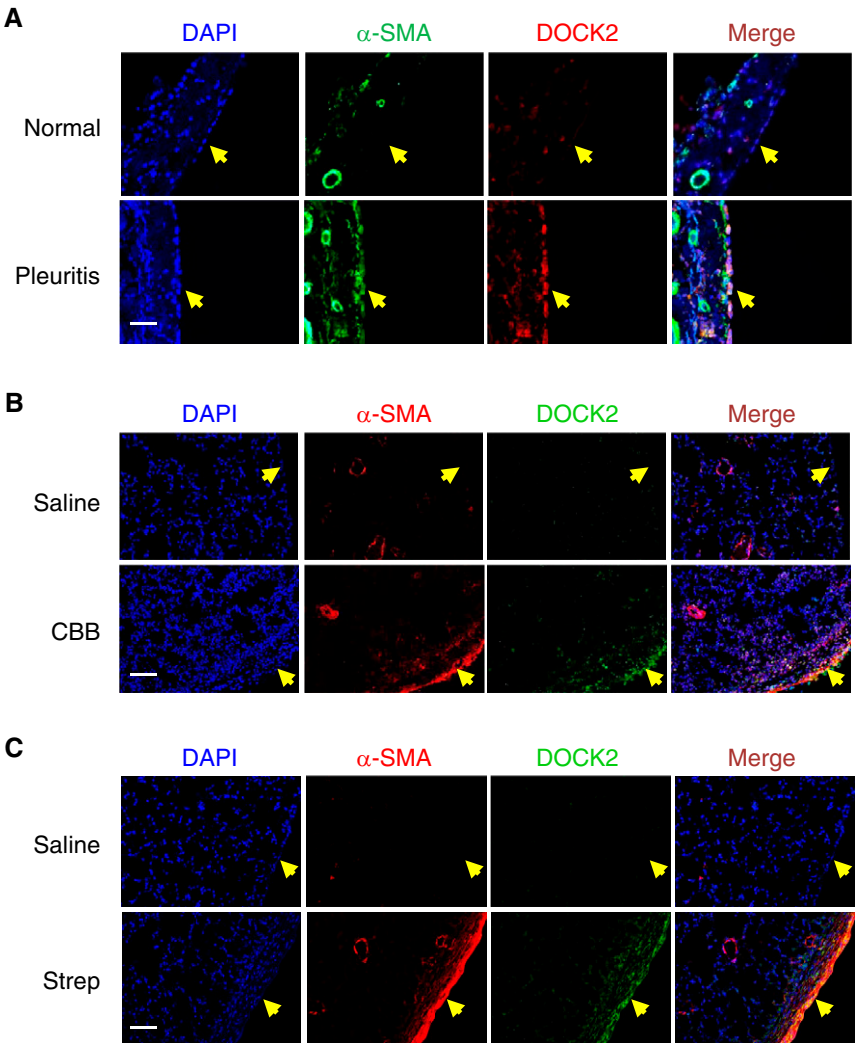

Figure 3. Colocalization of DOCK2 and α-SMA (α-smooth muscle actin) in pleural fibrosis *in vivo*. (*A*) IF staining of DOCK2 (red) and α-SMA (green) colocalization in human normal and pleuritis lung. (*B*) DOCK2 was induced and colocalized with the myofibroblast marker α-SMA (red) in lung tissues of C57BL/6 mice given CBB for 14 days. (*C*) IF staining showed DOCK2 (green) was induced and colocalized with myofibroblast marker α-SMA (red) in lung tissues of C57BL/6 mice given Strep for 14 days. Arrowheads indicate the DOCK2 (green), α-SMA (red), and colocalization (yellow) at the pleural surface. Scale bars, 100 μm.

in mediating MesoMT. Pretreatment with the DOCK2-Rac inhibitor CPYPP up to 5 μμM (higher concentrations induced cell death; data not shown) failed to suppress the induction of α-SMA induced by TGF-β (*see* Figure E5).

DOCK2 Mediates TGF-β–induced MesoMT Likely through Upregulating Snail

To further explore the potential mechanism by which DOCK2 regulates MesoMT, we tested whether TGF-β–induced DOCK2 affects the potent inducer of epithelial to mesenchymal transition, Snail, in the induction of MesoMT. The rationale for this line of analysis is mentioned in the beginning of the article. TGF-β significantly induced Snail expression in a dose-dependent manner at both protein and mRNA levels (Figures 7C and 7D). Knockdown of Snail significantly inhibited TGF-β–induced α-SMA expression at both protein and mRNA levels (Figures 7E and 7F and E6), suggesting the requirement of Snail in TGF-β–induced MesoMT.

Furthermore, DOCK2 knockdown significantly attenuated TGF-β–induced upregulation of Snail at both the protein and mRNA level (Figures 7G and 7H). Smad3 signaling is known to regulate the transcription of Snail (33). We furthermore sought to know whether DOCK2 affects Smad signaling. We found that knockdown of DOCK2 attenuates Smad3 and Smad2 activation induced by TGF-β (*see* Figures E7A and E7B). The use of the small molecular Smad3 inhibitor SIS3 also significantly inhibited the amount of TGF-β–induced Snail mRNA (*see* Figure E7C). Together, these data suggest that DOCK2 contributes to TGF-β–induced MesoMT through modulation of Snail expression in HMPCs, in part, via the Smad3 signaling pathway.

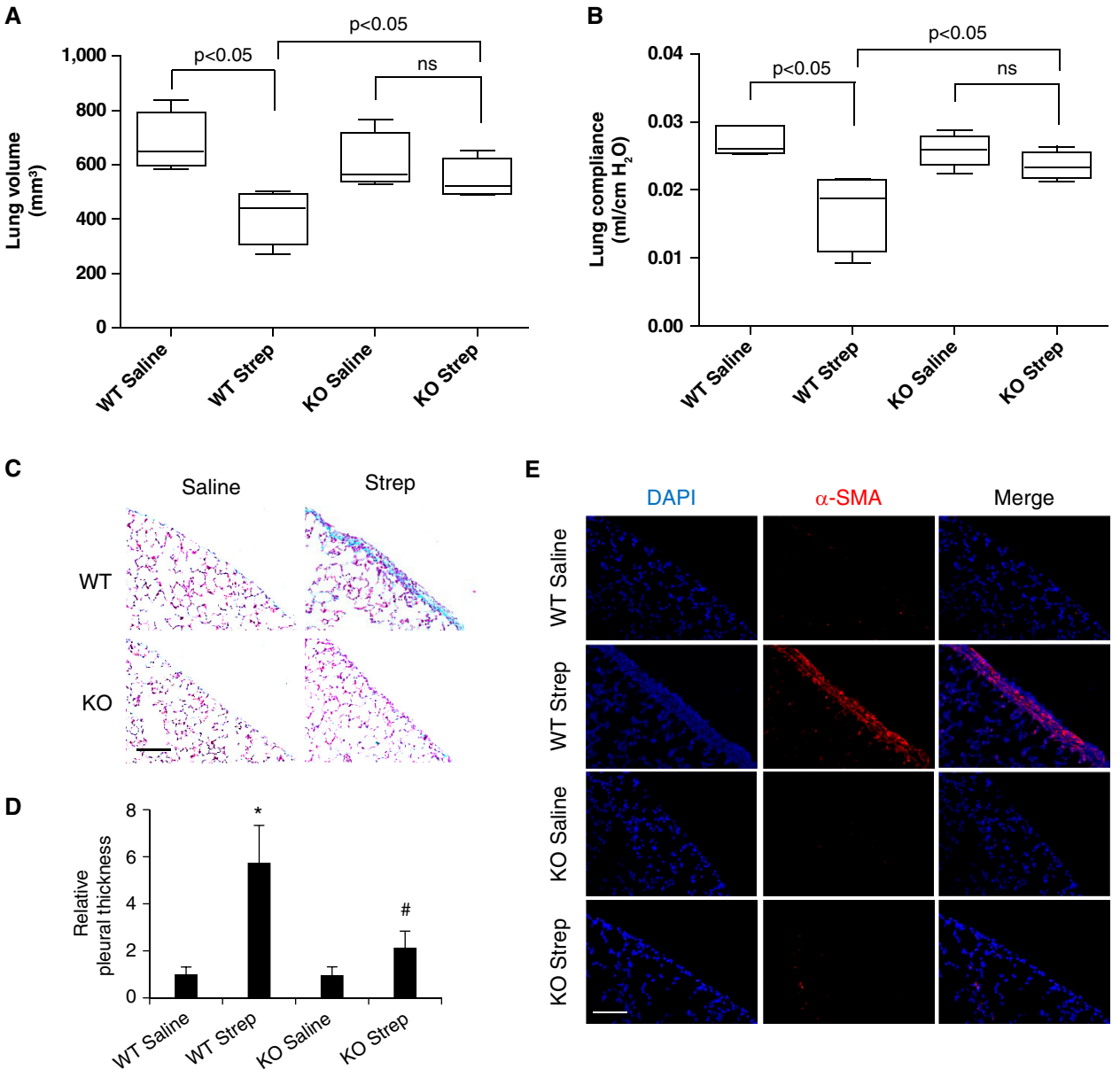

Figure 4. DOCK2-knockout (KO) mice were protected from Strep-induced pleural injury and impaired lung function. Wild-type (WT) C57BL/6 mice and DOCK2 KO mice were administered with 0.9% saline or Strep via intrapleural injection. (*A* and *B*) Seven days after treatment, lung volume (*A*) and lung function indicated by compliance (*B*) were examined through Micro CT and flexiVent, respectively. Boxplot was used to show the lung volume and compliance. (*C* and *E*) Lung tissues from these mice were collected for trichrome staining of collagen (*C*) and IF staining of the mesenchymal marker α-SMA (*E*). (*D*) Pleural thickness was measured using ImageJ software and compared. $n = 3$–5 mice per group, 15 fields per slide. Scale bars, 100 μm. $^{*}P < 0.05$ compared with WT saline and $^{\#}P < 0.05$ compared with WT strep. ns = not significant.

Discussion

The current study underscores an important role of DOCK2 in the pathogenesis of pleural fibrosis on the basis of several findings. DOCK2 is induced in the pleura in patients with human nonspecific pleuritis and *in vivo* models of induced pleural fibrosis. Expression of DOCK2 colocalized with α-SMA in lesions of pleural fibrosis. DOCK2 knockout blocked *S. pneumoniae*–induced pleural fibrosis *in vivo*. TGF-β induced DOCK2 expression in HPMCs, and knockdown of DOCK2 significantly attenuated TGF-β–induced MesoMT. To our knowledge, this is the first study to unveil an important role of DOCK2 in pleural fibrosis, extending understanding of its well-known function in regulating immunity.

PMCs may contribute to pleural injury and inappropriate repair through processes that involve both inflammatory and fibrotic cytokines and MesoMT (2, 8). Although other cell types may likewise contribute to

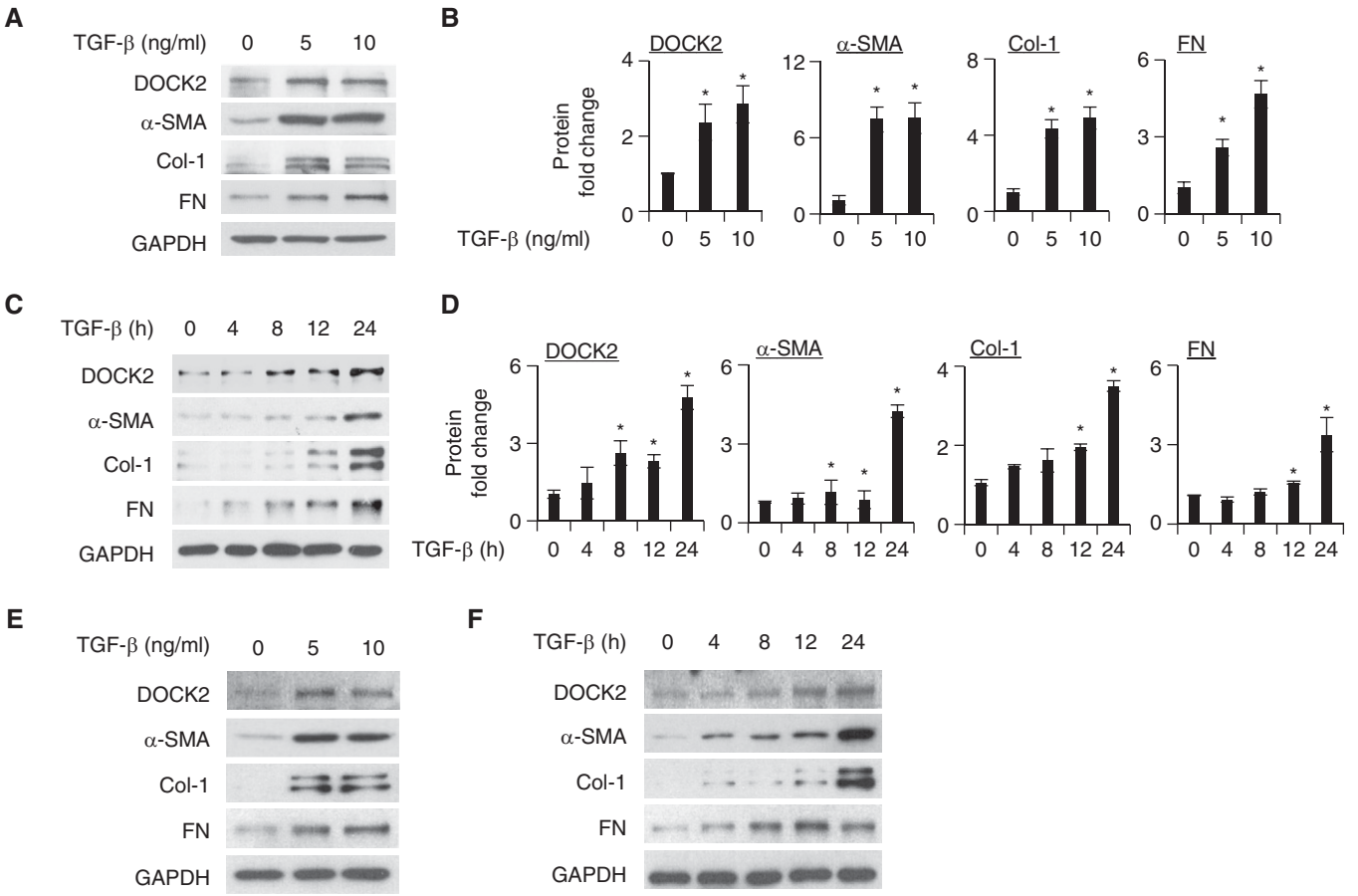

Figure 5. DOCK2 was induced in a dose- and time-dependent manner by TGF-β in human pleural mesothelial cells (HPMCs). (*A*) Serum-starved HPMCs were treated with TGF-β (0, 5, and 10 ng/ml) for 48 hours to detect DOCK2, α-SMA, collagen (Col-1), and fibronectin (FN) expression by western blotting (WB). GAPDH was a loading control. (*B*) Quantification of protein fold change as shown in (*A*). (*C*) Serum-starved HPMCs were treated with TGF-β (5 ng/ml) for various times (0, 4, 8, 12, and 24 h) to detect DOCK2, α-SMA, Col-1, and FN by WB with GAPDH as a loading control. (*D*) Quantification of protein fold change as shown in (*C*). (*E* and *F*) The induction of DOCK2 by TGF-β was confirmed in another line of HPMCs. The quantification was performed on the basis of data from three independent experiments. *$P < 0.05$ versus control group.

the pool of locally activated myofibroblasts, including fibroblasts, endothelial cells, and macrophages (34), PMCs undergoing MesoMT substantively contribute to the pool of activated myofibroblast within the injured pleural surfaces (35). In this study, patients with nonspecific pleuritis showed disorganized lung structure as well as increased collagen deposition (Figures 1A and 1B). Compared with the control patients, patients with nonspecific pleuritis showed notably increased expression of DOCK2 in the thickened mesothelial layer of the pleura (Figure 1C), which overlapped with that of α-SMA to a great extent (Figure 3A). These findings suggest that DOCK2 is proximately expressed in cells undergoing or transitioned to MesoMT. Further staining of pleural tissues with the mesothelial marker calretinin confirmed that DOCK2 induction was largely confined to mesothelial cells (*see* Figure E2). Together, these data offer proof of concept that DOCK2 contributes to the pathogenesis of this devastating disease, possibly through modulating MesoMT. It remains unclear, however, whether DOCK2 can serve as a predictive or prognostic marker for pleural fibrosis, which can be tested in well-controlled prospective studies in future.

While we were preparing this manuscript, another group reported that DOCK2 mediates LPS-induced macrophage inflammatory phenotype and acute parenchymal lung injury *in vivo* (23). However, the pathological role of DOCK2 in lung resident cells—for example, PMCs—was not addressed. In our present study, we found that DOCK2 was dramatically induced in the thickened pleural mesothelial layer indicative of fibrosis as induced by intrapleural administration of CBB, TGF-β, and *S. pneumoniae* infection (Figures 2 and 3), buttressing the concept that DOCK2 plays a role in the process of pleural remodeling. Furthermore, colocalization of DOCK2 and the myofibroblast marker α-SMA (Figure 3) in the pleural fibrosis models supports the idea that DOCK2 is induced in myofibroblasts and potentially contributes to the MesoMT. Moreover, the colocalization of DOCK2 with calretinin confirmed DOCK2 expression in the mesothelial cells (*see* Figure E2). Taken together, the data indicate that DOCK2 is induced in PMCs that expressed the MesoMT marker α-SMA, suggesting the

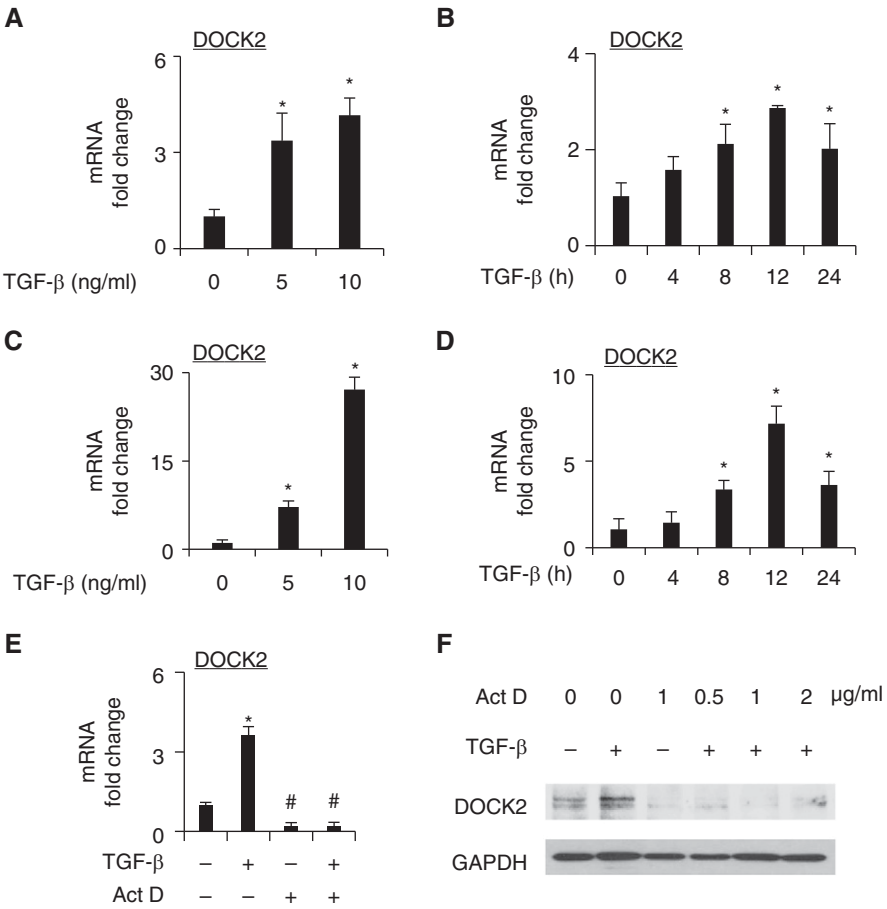

Figure 6. TGF-β induced DOCK2 expression at the transcriptional level in HPMCs. (*A*) Serum-starved HPMCs were treated with different doses of TGF-β (0, 5, and 10 ng/ml) for 12 hours to detect *DOCK2* mRNA by quantitative real-time PCR (qPCR). (*B*) Serum-starved HPMCs were treated with TGF-β (5 ng/ml) for various times (0, 4, 8, 12, and 24 h) to detect *DOCK2* mRNA expression by qPCR. (*C* and *D*) Experiments were conducted in another line of HPMCs, similar to experiments in *A* and *B*. (*E*) Serum-starved HPMCs were pretreated with actinomycin D (Act D, 1 μg/ml) for 30 minutes, followed by TGF-β (5 ng/ml) treatment for additional 6 hours to detect *DOCK2* mRNA expression by qPCR. The measurement was performed in triplicates. (*F*) Serum-starved HPMCs were pretreated with Act D (0.5–2 μg/ml) for 30 minutes, followed by TGF-β (5 ng/ml) treatment for an additional 12 hours to detect DOCK2 protein expression by WB with GAPDH as a loading control. $^{*}P < 0.05$ versus control group and $^{\#}P < 0.05$ versus TGF-β–treated group.

occurrence of MesoMT. Different *in vivo* models of pleural fibrosis may involve different mechanisms. However, DOCK2 expression was apparently and remarkably induced in pleural fibrosis in all the models examined in this study, suggesting that upregulation of DOCK2 might be a common and essential, pathophysiologically important event.

To determine the role of DOCK2 in pleural fibrosis development *in vivo*, we further treated WT and DOCK2-knockout mice with *S. pneumoniae* because it resembles human pneumonia-caused pleural injury and remodeling. We found that intrapleural injection of *S. pneumoniae* caused dramatic and significantly decreased lung volume and compliance, increased collagen deposition, and increased expression of the MesoMT marker α-SMA in the thickened pleural layer in WT mice (Figure 4). In contrast, DOCK2-knockout mice were protected from *S. pneumoniae*–induced abovementioned changes. These findings provide strong *in vivo* evidence that DOCK2 is crucial for the development of pleural fibrosis and was involved in the induction of MesoMT. Others have reported that lineage tracing of PMCs reveals important insight into the cell fate and their contribution to disease development (36–38). Future studies will eventually be performed in mice with labeled mesothelial cells and in conditional knockout mice to determine the kinetics of DOCK2 induction in mesothelial cells in our mouse models of pleural injury. Although these studies will help decipher the contribution of mesothelial cell DOCK2 expression, they currently lie outside of the scope of these studies, warranting future investigation.

TGF-β is one of the most potent inducers of MesoMT (5, 13) and was used to test whether DOCK2 is involved in regulation of MesoMT *in vitro*. As expected, TGF-β significantly induced DOCK2 expression time-dependently in two different primary HPMCs accompanying induction of α-SMA, collagen, and FN (Figure 5). DOCK2 was also noted to be significantly induced after 8-hour treatment with TGF-β, preceding that of mesenchymal markers of α-SMA, collagen, and FN, suggesting a potential role of DOCK2 in MesoMT.

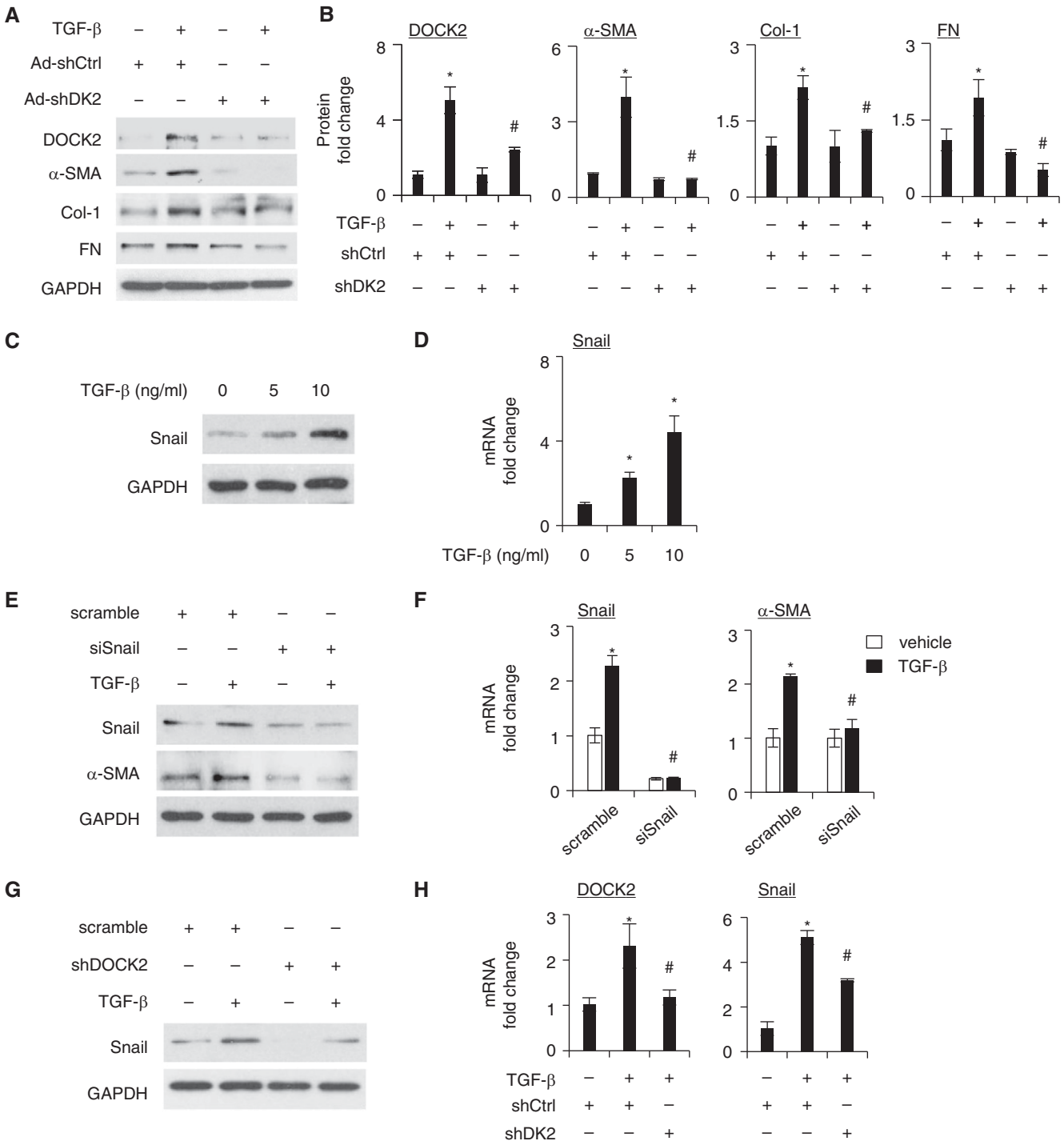

Figure 7. DOCK2 mediates TGF-β–induced MesoMT through snail pathway. (*A*) HPMCs were infected with adenovirus control or DOCK2 shRNA and then treated with TGF-β (5 ng/ml) for 24 hours to detect DOCK2, α-SMA, Col-1, and FN by WB. GAPDH was a loading control. (*B*) Quantification of protein fold change as shown in (*A*). The quantification was performed on the basis of data from three independent experiments. (*C* and *D*) Serum-starved HPMCs were treated with different doses of TGF-β (0, 5, and 10 ng/ml) for 24 hours to detect protein expression of Snail by WB (*C*) or for 12 hours to detect mRNA expression of Snail by qPCR (*D*). (*E* and *F*) HPMCs were transfected with scramble or Snail siRNA (siSnail), followed by TGF-β treatment (10 ng/ml) for 24 hours to detect Snail and α-SMA expression by WB (*E*) or for 12 hours to detect mRNA by qPCR (*F*). (*G*) HPMCs were transfected with scramble or siSnail, followed by TGF-β treatment (10 ng/ml) for 24 hours to detect Snail protein expression. (*H*) HPMCs were transfected with scramble or siSnail, followed by TGF-β treatment (10 ng/ml) for 12 hours to detect mRNA expression of DOCK2 and Snail by qPCR. GAPDH was used as an internal control for these qPCR analyses. $n = 3$ replicates for each treatment in qPCR analysis. $^{*}P < 0.05$ versus control group and $^{\#}P < 0.05$ versus TGF-β–treated adenovirus control group. Ad-shCtrl = adenovirus control shRNA; Ad-shDK2 = adenovirus DOCK2 shRNA.

DOCK2 has previously been reported to express in only hematopoietic cells to regulate lymphocyte migration (25, 39). Increasing evidence demonstrates that DOCK2 can be induced by different cytokines (22, 24) including PDGF, TNF-α, and IL-1β. A previous RNA-sequencing study showed that DOCK2 is among the most upregulated genes because of treatment with TGF-β (10 ng/ml) in the lung adenocarcinoma cell line A549 (40), although no functional assay is involved regarding the role of DOCK2. Consistently, our study also showed that TGF-β induces DOCK2 mRNA expression in two different primary HPMCs, which can be blocked by the transcription inhibitor Act D (Figure 6), further confirming the transcriptional regulation of DOCK2 by TGF-β.

Next, we tested whether DOCK2 is required for TGF-β–induced MesoMT in HPMCs. We infected HPMCs with control or shDOCK2 adenovirus and then stimulated the cells with saline or TGF-β. DOCK2 knockdown successfully abolished/attenuated TGF-β–induced α-SMA, Col-1, and FN expression (Figures 7A and 7B). The data support an important role of DOCK2 in mediating TGF-β–induced MesoMT. We also tested whether the DOCK2-Rac1 inhibitor CPYPP could block TGF-β–induced MesoMT (Figure E5). Although these data are negative, the *in vitro* half-maximal inhibitory concentration of CPYPP for inhibiting Rac1 was reported to be >20 μμM, and the spleen cells were viable in the presence of 100 μμM CPYPP for 3 days (28). In contrast, doses >5 μμM were cytotoxic in our model system (data not shown). Unfortunately, no other validated DOCK2-Rac1 GEF (guanine nucleotide exchange factor) inhibitor is available. As such, we believe that the results are inconclusive and additional studies that are out of the scope of this work are required to address this issue.

Snail is an important transcriptional factor that drives epithelial to mesenchymal transition in cancer (41, 42) and MesoMT in peritoneal fibrosis (43–45). However, whether it is involved in mediating pleural MesoMT remains unclear. We found here that TGF-β dose-dependently induced Snail expression in HPMCs (Figures 7C and 7D). Snail was not only induced by TGF-β but also required for TGF-β–induced MesoMT (Figures 7E, 7F, and E6). Interestingly, DOCK2 knockdown significantly attenuated TGF-β–induced Snail upregulation in HPMCs (Figures 7G and 7H). Snail has been reported to be transcriptionally regulated by Smad3 during epithelial to mesenchymal transition (33). In this study, we confirmed that inhibition of Smad3 with the specific inhibitor SIS3 significantly attenuated TGF-β–induced Snail expression (Figure E7C). Interestingly, DOCK2 knockdown also inhibited the activation of Smad3 and Smad2 in HPMCs (Figures E7A and E7B). These data together suggest that DOCK2 may upregulate Snail to mediate TGF-β–induced MesoMT in HPMCs at least partly dependent on the Smad3 pathway. Generation of Snail-knockout cells would be helpful to confirm the essential role of Snail in TGF-β–induced MesoMT. However, this approach could not be achieved in our primarily cultured mesothelial cells as we only use the first five passages to maintain their phenotype and response to TGF-β stimulus.

In summary, we report a newly recognized contribution of DOCK2 to the pathogenesis of organizing pleural injury and fibrosis on the basis of patient data and those obtained from preclinical models of organizing pleural injury. The induction of DOCK2 in primary HPMCs that undergo MesoMT and the attenuated effect of TGF-β to induce MesoMT with DOCK2 knockdown suggest that DOCK2 acts to regulate MesoMT to promote pleural fibrosis. Future study is warranted to test whether targeting of DOCK2 after induction of pleural injury can protect against the development of subsequent lung restriction, pleural fibrosis, and fibrothorax. ■

Author disclosures are available with the text of this article at www.atsjournals.org.

References

1. Huggins JT, Sahn SA. Drug-induced pleural disease. *Clin Chest Med* 2004;25:141–153.
2. Mutsaers SE, Prele CM, Brody AR, Idell S. Pathogenesis of pleural fibrosis. *Respirology* 2004;9:428–440.
3. Decologne N, Wettstein G, Kolb M, Margetts P, Garrido C, Camus P, *et al.* Bleomycin induces pleural and subpleural fibrosis in the presence of carbon particles. *Eur Respir J* 2010;35:176–185.
4. Tucker TA, Jeffers A, Alvarez A, Owens S, Koenig K, Quaid B, *et al.* Plasminogen activator inhibitor-1 deficiency augments visceral mesothelial organization, intrapleural coagulation, and lung restriction in mice with carbon black/bleomycin-induced pleural injury. *Am J Respir Cell Mol Biol* 2014;50:316–327.
5. Tucker T, Tsukasaki Y, Sakai T, Mitsuhashi S, Komatsu S, Jeffers A, *et al.* Myocardin is involved in mesothelial-mesenchymal transition of human pleural mesothelial cells. *Am J Respir Cell Mol Biol* 2019;61:86–96.
6. Tucker TA, Jeffers A, Boren J, Quaid B, Owens S, Koenig KB, *et al.* Organizing empyema induced in mice by Streptococcus pneumoniae: effects of plasminogen activator inhibitor-1 deficiency. *Clin Transl Med* 2016;5:17.
7. Tucker T, Idell S. Plasminogen-plasmin system in the pathogenesis and treatment of lung and pleural injury. *Semin Thromb Hemost* 2013;39: 373–381.
8. Komissarov AA, Rahman N, Lee YCG, Florova G, Shetty S, Idell R, *et al.* Fibrin turnover and pleural organization: bench to bedside. *Am J Physiol Lung Cell Mol Physiol* 2018;314:L757–L768.
9. Koopmans T, Rinkevich Y. Mesothelial to mesenchyme transition as a major developmental and pathological player in trunk organs and their cavities. *Commun Biol* 2018;1:170.
10. Mutsaers SE, Birnie K, Lansley S, Herrick SE, Lim CB, Prêle CM. Mesothelial cells in tissue repair and fibrosis. *Front Pharmacol* 2015; 6:113.
11. Scotton CJ, Krupiczojc MA, Königshoff M, Mercer PF, Lee YC, Kaminski N, *et al.* Increased local expression of coagulation factor X contributes to the fibrotic response in human and murine lung injury. *J Clin Invest* 2009;119:2550–2563.
12. Glauser FL, Otis PT, Levine RI, Smith WR. Coagulation factors and fibrinogen in pleural effusions. *Respiration* 1976;33: 396–402.
13. Owens S, Jeffers A, Boren J, Tsukasaki Y, Koenig K, Ikebe M, *et al.* Mesomesenchymal transition of pleural mesothelial cells is PI3K and NF-κB dependent. *Am J Physiol Lung Cell Mol Physiol* 2015;308: L1265–L1273.
14. Gauldie J, Bonniaud P, Sime P, Ask K, Kolb M. TGF-beta, Smad3 and the process of progressive fibrosis. *Biochem Soc Trans* 2007;35: 661–664.
15. Boren J, Shryock G, Fergis A, Jeffers A, Owens S, Qin W, *et al.* Inhibition of glycogen synthase kinase 3β blocks mesomesenchymal transition and attenuates streptococcus pneumonia-mediated pleural injury in mice. *Am J Pathol* 2017;187:2461–2472.
16. Wendt MK, Tian M, Schiemann WP. Deconstructing the mechanisms and consequences of TGF-β-induced EMT during cancer progression. *Cell Tissue Res* 2012;347:85–101.

17. Guo X, Jose PA, Chen SY. Response gene to complement 32 interacts with Smad3 to promote epithelial-mesenchymal transition of human renal tubular cells. *Am J Physiol Cell Physiol* 2011;300:C1415–C1421.
18. Reif K, Cyster J. The CDM protein DOCK2 in lymphocyte migration. *Trends Cell Biol* 2002;12:368–373.
19. Hanawa-Suetsugu K, Kukimoto-Niino M, Mishima-Tsumagari C, Akasaka R, Ohsawa N, Sekine S, *et al.* Structural basis for mutual relief of the Rac guanine nucleotide exchange factor DOCK2 and its partner ELMO1 from their autoinhibited forms. *Proc Natl Acad Sci USA* 2012; 109:3305–3310.
20. Chang L, Yang J, Jo CH, Boland A, Zhang Z, McLaughlin SH, *et al.* Structure of the DOCK2-ELMO1 complex provides insights into regulation of the auto-inhibited state. *Nat Commun* 2020;11:3464.
21. Guo X, Chen SY. Dedicator of cytokinesis 2 in cell signaling regulation and disease development. *J Cell Physiol* 2017;232:1931–1940.
22. Guo X, Shi N, Cui XB, Wang JN, Fukui Y, Chen SY. Dedicator of cytokinesis 2, a novel regulator for smooth muscle phenotypic modulation and vascular remodeling. *Circ Res* 2015;116:e71–e80.
23. Xu X, Su Y, Wu K, Pan F, Wang A. DOCK2 contributes to endotoxemia-induced acute lung injury in mice by activating proinflammatory macrophages. *Biochem Pharmacol* 2021;184:114399.
24. Guo X, Li F, Xu Z, Yin A, Yin H, Li C, *et al.* DOCK2 deficiency mitigates HFD-induced obesity by reducing adipose tissue inflammation and increasing energy expenditure. *J Lipid Res* 2017;58:1777–1784.
25. Fukui Y, Hashimoto O, Sanui T, Oono T, Koga H, Abe M, *et al.* Haematopoietic cell-specific CDM family protein DOCK2 is essential for lymphocyte migration. *Nature* 2001;412:826–831.
26. Idell S, Zwieb C, Kumar A, Koenig KB, Johnson AR. Pathways of fibrin turnover of human pleural mesothelial cells in vitro. *Am J Respir Cell Mol Biol* 1992;7:414–426.
27. Qian G, Yao W, Zhang S, Bajpai R, Hall WD, Shanmugam M, *et al.* Co-inhibition of BET and proteasome enhances ER stress and Bim-dependent apoptosis with augmented cancer therapeutic efficacy. *Cancer Lett* 2018;435:44–54.
28. Nishikimi A, Uruno T, Duan X, Cao Q, Okamura Y, Saitoh T, *et al.* Blockade of inflammatory responses by a small-molecule inhibitor of the Rac activator DOCK2. *Chem Biol* 2012;19:488–497.
29. Qian G, Wang D, Magliocca KR, Hu Z, Nannapaneni S, Kim S, *et al.* Human papillomavirus oncoprotein E6 upregulates c-Met through p53 downregulation. *Eur J Cancer* 2016;65:21–32.
30. Qin W, Jeffers A, Owens S, Chauhan P, Komatsu S, Qian G, *et al.* NOX1 promotes mesothelial-mesenchymal transition through modulation of reactive oxygen species-mediated signaling. *Am J Respir Cell Mol Biol* 2021;64:492–503.
31. Nasreen N, Mohammed KA, Mubarak KK, Baz MA, Akindipe OA, Fernandez-Bussy S, *et al.* Pleural mesothelial cell transformation into myofibroblasts and haptotactic migration in response to TGF-beta1 in vitro. *Am J Physiol Lung Cell Mol Physiol* 2009;297:L115–L124.
32. Barberis MC, Faleri M, Veronese S, Casadio C, Viale G. Calretinin. A selective marker of normal and neoplastic mesothelial cells in serous effusions. *Acta Cytol* 1997;41:1757–1761.
33. Peinado H, Quintanilla M, Cano A. Transforming growth factor beta-1 induces snail transcription factor in epithelial cell lines: mechanisms for epithelial mesenchymal transitions. *J Biol Chem* 2003;278: 21113–21123.
34. Yazdani S, Bansal R, Prakash J. Drug targeting to myofibroblasts: implications for fibrosis and cancer. *Adv Drug Deliv Rev* 2017;121: 101–116.
35. Yang AH, Chen JY, Lin JK. Myofibroblastic conversion of mesothelial cells. *Kidney Int* 2003;63:1530–1539.
36. Karki S, Surolia R, Hock TD, Guroji P, Zolak JS, Duggal R, *et al.* Wilms' tumor 1 (Wt1) regulates pleural mesothelial cell plasticity and transition into myofibroblasts in idiopathic pulmonary fibrosis. *FASEB J* 2014;28: 1122–1131.
37. Zolak JS, Jagirdar R, Surolia R, Karki S, Oliva O, Hock T, *et al.* Pleural mesothelial cell differentiation and invasion in fibrogenic lung injury. *Am J Pathol* 2013;182:1239–1247.
38. Li Y, Lua I, French SW, Asahina K. Role of TGF-β signaling in differentiation of mesothelial cells to vitamin A-poor hepatic stellate cells in liver fibrosis. *Am J Physiol Gastrointest Liver Physiol* 2016;310: G262–G272.
39. Nishihara H, Kobayashi S, Hashimoto Y, Ohba F, Mochizuki N, Kurata T, *et al.* Non-adherent cell-specific expression of DOCK2, a member of the human CDM-family proteins. *Biochim Biophys Acta* 1999;1452: 179–187.
40. Li Y, Rouhi O, Chen H, Ramirez R, Borgia JA, Deng Y. RNA-seq and network analysis revealed interacting pathways in TGF-β-treated lung cancer cell lines. *Cancer Inform* 2015;13:129–140.
41. Barrallo-Gimeno A, Nieto MA. The Snail genes as inducers of cell movement and survival: implications in development and cancer. *Development* 2005;132:3151–3161.
42. Cano A, Pérez-Moreno MA, Rodrigo I, Locascio A, Blanco MJ, del Barrio MG, *et al.* The transcription factor snail controls epithelial-mesenchymal transitions by repressing E-cadherin expression. *Nat Cell Biol* 2000;2: 76–83.
43. Yáñez-Mó M, Lara-Pezzi E, Selgas R, Ramírez-Huesca M, Domínguez-Jiménez C, Jiménez-Heffernan JA, *et al.* Peritoneal dialysis and epithelial-to-mesenchymal transition of mesothelial cells. *N Engl J Med* 2003;348:403–413.
44. Miyake T, Sakai N, Tamai A, Sato K, Kamikawa Y, Miyagawa T, *et al.* Trehalose ameliorates peritoneal fibrosis by promoting Snail degradation and inhibiting mesothelial-to-mesenchymal transition in mesothelial cells. *Sci Rep* 2020;10:14292.
45. López-Cabrera M. Mesenchymal conversion of mesothelial cells is a key event in the pathophysiology of the peritoneum during peritoneal dialysis. *Adv Med* 2014;2014:473134.